Test Results of Superconducting Combined Function Prototype Magnets for the J-PARC Neutrino Beam Line

Ken-ichi Sasaki, Tatsushi Nakamoto, Norio Higashi, Nobuhiro Kimura, Yasuo Ajima, Toru Ogitsu, Takayuki Tomaru, Masahisa Iida, Hirokatsu Ohhata, Shigekatsu Sugawara, Ken-ichi Tanaka, Yasuhiro Makida, Takahiro Okamura, Osamu Araoka, Katsuyu Kasami, Akira Yamamoto

***Abstract*— Superconducting combined function magnets are adopted for the 50 GeV, 750 kW proton beam line for the J-PARC neutrino experiment, and two full-scale prototype magnets have been developed successfully at KEK. In the cold tests, both prototypes were excited up to 7700 A without spontaneous quenches. The measured field quality of the both prototypes agreed well with the design field, indicating that the fabrication process has no major problem. The heater quench tests of the first prototype, however, showed that the magnet was not self-protected. Consequently, the design was revised and quench protection heaters were adopted. In quench heater tests of the second prototype magnet using small sheet heaters, the fundamental characteristics of the quench protection heaters were studied.**

***Index Terms*— J-PARC, Neutrino, Superconducting Combined Function Magnet, Magnetic Field Measurement, Quench Protection Heater.**

I. Introduction

A next generation long-baseline neutrino oscillation experiment is planned to study the fundamental nature of neutrinos [1], [2]. It will require the proton beam extracted from J-PARC 50 GeV, 0.75 MW proton accelerator jointly built by JAERI and KEK. The beam line which guides the proton beam to the production target of secondary particles consists of 28 superconducting combined function magnets, SCFMs, currently developed at KEK.

The unique feature of the magnet design is a left-right asymmetric structure. A cross section of the magnet and an enlarged view of the half coil are shown in Fig 1. The magnets have a large aperture of 173.4 mm, a magnetic length of 3.3 m and an outer diameter of 570 mm. The current distribution which generates both dipole field of 2.6 T and quadrupole field of 19 T/m with a current of 7345 A, is combined into a single layer coil. The coil is encased in the glass-fiber reinforced phenolic plastic collars surrounded by an iron yoke. The yoke design is based on the CERN-LHC IR Quadrupole magnet, MQXA, developed at KEK [3]. The use of the plastic collar instead of conventional metallic collars and the design transferred from MQXA reduce fabrication costs.

Manuscript received September 20, 2005.

Ken-ichi Sasaki, Tatsushi Nakamoto, Norio Higashi, Nobuhiro Kimura, Yasuo Ajima, Toru Ogitsu, Takayuki Tomaru, Masahisa Iida, Hirokatsu Ohhata, Shigekatsu Sugawara, Ken-ichi Tanaka, Yasuhiro Makida, Takahiro Okamura, Osamu Araoka, Katsuyu Kasami and Akira Yamamoto are with the High Energy Accelerator Research Organization (KEK), 1-1 Oho, Tsukuba, 305-0801 Japan (e-mail:ken-ichi.sasaki@kek.jp).

Two full-scale prototypes of SCFMs have been developed successfully at KEK. The first prototype magnet is to confirm the magnet design and fabrication tools, and the second prototype magnet is to verify the technology transfer to an industrial company and the reproducibility of the manufacturing process. The details on the design and development of SCFMs are described in the previous papers [4]-[7]. This paper reports the results of cold tests of the first and second prototype magnets. In addition, the revision of quench protection scheme is reported.

II. Results of Excitation Tests

The cold test was performed in liquid helium at 4.2 K in a vertical cryostat with an inner diameter of 720 mm and 9 m depth, which was used for testing of LHC-MQXA magnets. Fig. 2 shows the installation of the magnet into the vertical cryostat. After the first cold test, the first prototype magnet was once warmed up to room temperature, then cooled again and the second cold test was carried out.

After nine manually switched-off tests at the power supply current gradually increased for checking the system, the first prototype magnet was ramped up at 5 A/s and successfully reached 7700 A, the current limit of the power supply, without spontaneous quenches, It sufficiently exceeds the operational current of 7345 A at the expected maximum proton beam energy of 50 GeV. Fast ramp tests up to the nominal current of 7345 A were also conducted with different ramp rates, although the magnet will be operated only in DC mode. The magnet did not quench even at the maximum ramp rate of 1000 A/s corresponding to the ramp rate limit of the power supply, indicating that AC losses in the magnet are small. During the fast ramp up/down tests, the inductance of the magnet was measured. The inductance derived from inductive voltage of the magnet was about 14.2 mH which is close to the design value of 14.3 mH.

In the second cold test, the magnet was energized up again to 7700 A without spontaneous quenches, and other test results were the same as that in the first cold test. Namely, no thermal cycle effect was observed on the magnet performance.

The second prototype magnet had the same excitation tests as the first prototype. It was energized to the current of 7700 A without a spontaneous quench, too. The fast ramp tests were also conducted, and the magnet experienced the first

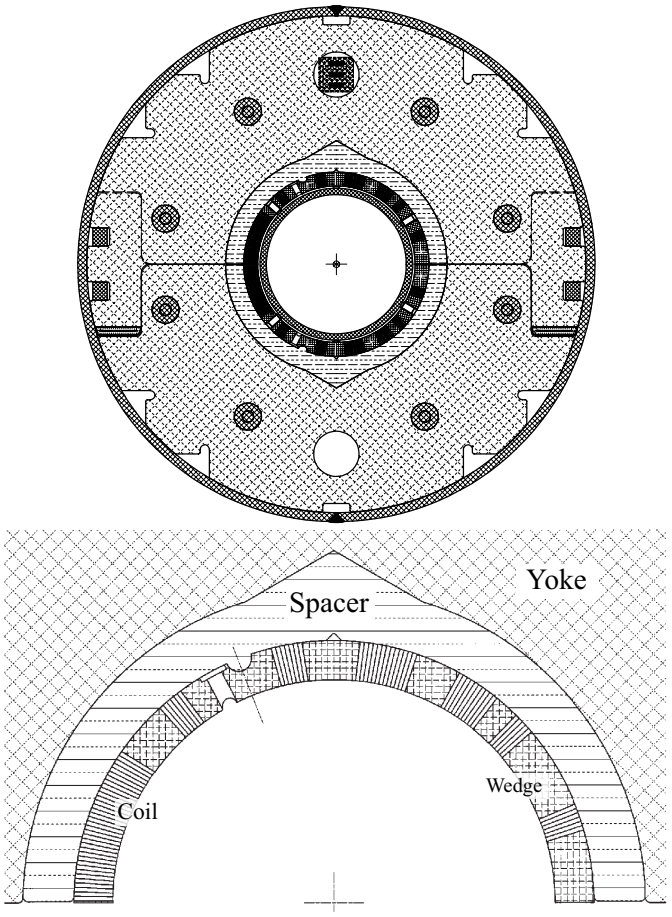

Fig. 1. Cross section of the superconducting combined function magnet viewed from the lead end (top), and enlarged view of the coil (bottom). The coil aperture diameter is 173.4 mm.

spontaneous quench at 6453 A with 1000 A /s. This magnet didn't have the voltage taps to identify the position of quench origin, therefore, it can be only found that the quench started in the lower half of the coil cross section. However, since the magnet is limited to DC application, it does not affect on the basic magnet performance. The magnet inductance measured during the fast ramp tests was about 14.3 mH, corresponding to the design value.

III. Magnetic Field Measurement

A. Measurement System

The magnetic field measurements were performed with a rotating probe. The rotating probe consists of five radial coils with rectangular shape, about 20 mm wide and 500 mm long that are printed and placed in parallel on a circuit board by an etching method. Each coil has 20 turns. The rotating probe can move along the magnet axis in the warm bore of the vertical cryostat to perform longitudinal scans. Analog bucked signals to reduce dipole and quadrupole components were taken by using a precise digital integrator, that was triggered by an angular encoder. The harmonics field is derived from Fourier coefficients of integrator readouts.

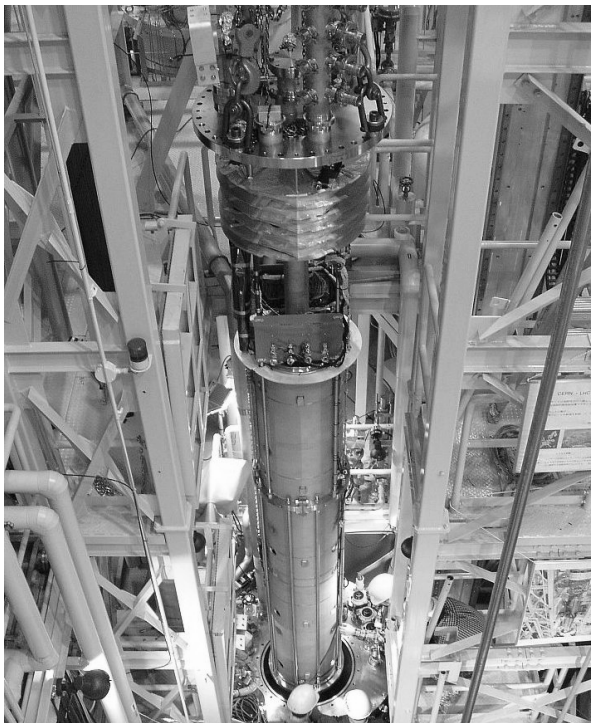

Fig. 2. Prototype magnet installation into the vertical cryostat.

B. Definition of Multipole Components

The multipole field components are described as the multipole coefficients at a reference radius, r_0, of 50 mm by the equation 1,

$$B_y + iB_x = \sum_{n=1}^{\infty} (B_n + iA_n) \left(\frac{x+iy}{r_0} \right)^{(n-1)}, \qquad (1)$$

where B_n, A_n are the normal and the skew 2n-pole field components (in Tesla), respectively.

A main concern about the field measurement of combined function magnets, is the position of the rotating axis of the probes. The magnet is hanged in a vertical cryostat during the cold test, and it is very difficult to coincide the axis of rotation with the magnet central axis. This fact makes it difficult to determine the dipole field with good accuracy in the SCFM. Because SCFM generates both the dipole and quadrupole fields, and "feed down" of quadrupole field affects on the amplitude of dipole signal. In the following analysis, the angular compensation is only adopted so that the skew quadrupole component along the straight section might be fit into zero. The exact dipole field will be measured at the horizontal test stand for the several production magnets. The warm measurement at the horizontal test bench are reported in [8].

C. Results

Table I summarizes the field quality in the magnet straight section at currents corresponding to 40 GeV and 50 GeV. The measured results are compared with the computed results in Table I. The computation is made using Opera2D. The measured field strength of the quadrupole field is in a good

TABLE I
FIELD QUALITY OF THE SCFM IN THE STRAIGHT SECTION AT THE REFERENCE RADIUS OF 5 CM

	Measured		Computed	
Multipole	@5921 A	@7460 A	@5921 A	@7460 A
B_1(T)	2.14	2.68	2.101	2.624
B_2(T)	0.76	0.95	0.764	0.949
$B_3(10^{-4}\mathrm{T})$	9.3	16.5	4.3	3.4
$B_4(10^{-4}\mathrm{T})$	0.3	25.6	0.3	25.7
$B_5(10^{-4}\mathrm{T})$	− 5.4	0.2	1.7	7.4
$B_6(10^{-4}\mathrm{T})$	−14.4	−19.6	−12.6	−16.5
$B_7(10^{-4}\mathrm{T})$	− 7.3	−11.6	− 1.1	− 2.4
$B_8(10^{-4}\mathrm{T})$	−18.0	−24.5	− 7.8	− 9.9
$B_9(10^{-4}\mathrm{T})$	−20.2	−25.7	−18.6	−23.4
$B_{10}(10^{-4}\mathrm{T})$	− 3.8	− 5.1	− 0.5	− 0.7
$B_{11}(10^{-4}\mathrm{T})$	− 3.0	− 3.1	− 6.3	− 8.0
$B_{12}(10^{-4}\mathrm{T})$	4.9	6.2	4.3	5.4

TABLE II
INTEGRAL FIELD QUALITY OF THE SCFM AT THE REFERENCE RADIUS OF 5 CM

	Measured		Computed	
Multipole	@5921 A	@7460 A	@5921 A	@7460 A
B_1(T·m)	7.097	8.906	7.060	8.841
B_2(T·m)	2.510	3.127	2.539	3.164
$B_3(10^{-4}\mathrm{T{\cdot}m})$	−187.1	−220.6	−240.2	−299.4
$B_4(10^{-4}\mathrm{T{\cdot}m})$	− 68.4	− 5.9	− 65.1	− 12.7
$B_5(10^{-4}\mathrm{T{\cdot}m})$	− 59.2	− 51.9	− 41.4	− 28.2
$B_6(10^{-4}\mathrm{T{\cdot}m})$	− 55.8	− 75.2	− 49.2	− 63.8
$B_7(10^{-4}\mathrm{T{\cdot}m})$	− 29.8	− 44.6	− 15.0	− 21.4
$B_8(10^{-4}\mathrm{T{\cdot}m})$	− 54.9	− 74.5	− 25.6	− 32.5
$B_9(10^{-4}\mathrm{T{\cdot}m})$	− 62.9	− 79.9	− 59.3	− 74.6
$B_{10}(10^{-4}\mathrm{T{\cdot}m})$	− 10.1	− 13.8	− 0.3	− 0.3
$B_{11}(10^{-4}\mathrm{T{\cdot}m})$	− 9.9	− 10.9	− 20.6	− 25.9
$B_{12}(10^{-4}\mathrm{T{\cdot}m})$	18.9	13.2	13.4	16.8

agreement with the computation, although there is a small discrepancy in the dipole field. It may be induced by the alignment error of the measurement system with respect to the magnet center as described above. The estimated alignment error is about 2.5 mm, which is presumable from the measurement system tolerances. The change in higher order multipole coefficients from 40 GeV to 50 GeV is small except for the octupole coefficient consistently observed in the measured results.

The integral field quality of the magnet is summarized in Table II. The computed results are obtained using Opera3D. The measured results generally agree with computed results. Since the field quality around the coil ends is not as good as that in the straight section due to limited optimization of the single layer coil structure, the magnitude of higher order harmonics was relatively large. However, the beam simulations indicate that such field quality is acceptable for the primary proton beam line extracted for the J-PARC neutrino experiment.

The field measurements of the second prototype were performed using the same system as for the first prototype. The field quality in the straight section and the integrated field of the second prototype magnet are given in Fig. 3 and 4, respectively. The figures in parentheses represent dipole and quadrupole components. In the both straight section and integral field, there were no major discrepancies between the first and the second prototype. The second prototype has been fabricated with the same design and fabrication process as the first prototype. Namely, the measured results indicate that the reproducibility of the magnet fabrication is good enough, and the fabrication technology was successfully transferred to the company.

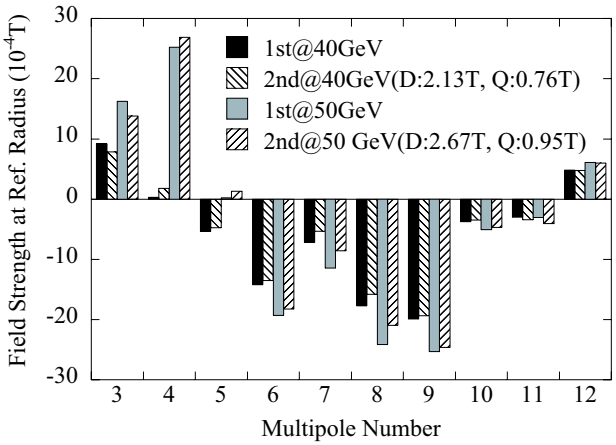

Fig. 3. Field strength at the reference radius of 5 cm of the second prototype magnet. The results of the first prototype magnet are also plotted for comparison. The figures in parentheses represent dipole and quadrupole components at 5920 A and 7460 A.

IV. QUENCH HEATER TESTS

A. Results of the First Prototype

The first prototype magnet is equipped with 57 voltage taps and 6 quench-inducing heaters to observe the quench characteristics. The magnetic field distribution on the conductors is asymmetric due to the unique coil structure, the field on the left side is higher than the right side in Fig. 1. The quench-inducing heaters are attached to both the top and bottom coils at three positions: at the 7th turn of the high field side, 36th turn in the low field side, and at the lead end on the median plane in the lowest field region. These heaters can induce quench in a single turn. Most voltage taps are attached in proximity to the heaters so that the initial quench propagation can be observed. In the quench tests, the dump resistor of 50 mΩ instead of the cold diode was connected in parallel to the coil circuit. The power supply was shut down when the magnet balance voltage exceeded a threshold of the quench detector.

The balanced voltage rises of the magnet at currents of 7345 A and 5830 A are shown in Fig. 5. The voltage rise, when the heater located at the lower field was fired was much slower than for the higher field case. This is caused by the difference of quench propagation velocity at each magnetic field. Fig. 6 shows the quench propagation velocities as a function of distance from quench heater. The symbol represents the average quench propagation velocity within the segment indicated by the dotted lines. The velocity in the lower field region is very slow, especially, the velocity around the lead is about 2 m/s mainly because of the large quench margin of the cable. The calculated magnetic field around the heater at the lead is about 0.8 T at 7345 A, the I/Ic ratio is expected to be only about 0.04.

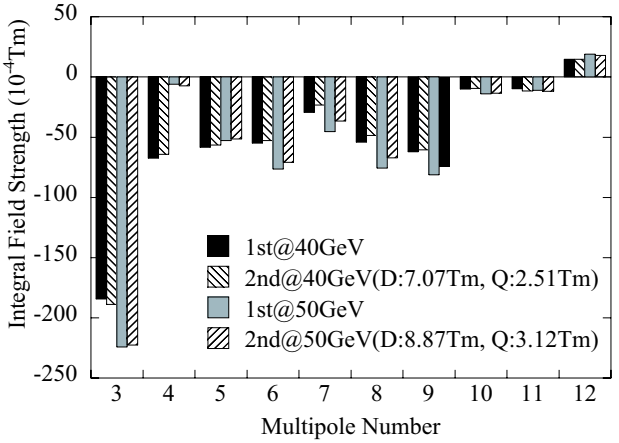

Fig. 4. Integral field quality at the reference radius of 5 cm of the second prototype magnet. The results of the first prototype magnet are also plotted for comparison. The figures in parentheses represent dipole and quadrupole components at 5920 A and 7460 A.

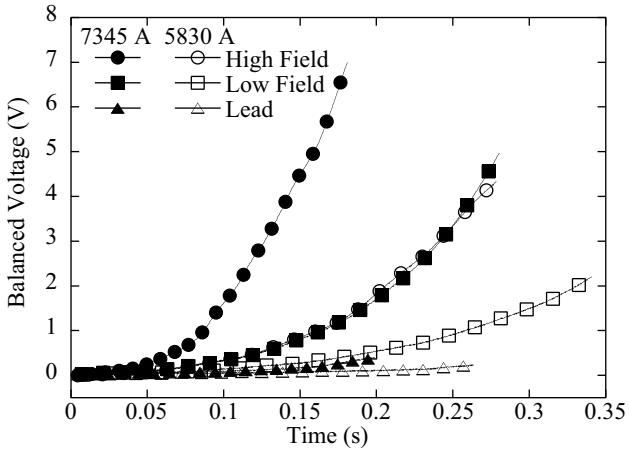

Fig. 5. Measured balanced voltage rise during the heater quench tests at the currents corresponding to 50 GeV and 40 GeV. t = 0 s is the start time of the quench.

B. Numerical Simulation of Quench Protection

In the initial protection scheme, the magnets are protected only by the cold diode connected in parallel to each magnet [5]. Under a normal operating condition, the diode is cooled to the liquid helium temperature, and the turn on voltage of the diode is expected to be 6 V. Since the magnet voltage is considerably lower than the turn-on voltage, the current does not flow into the diode. Once the quench occurs and propagates, the magnet terminal voltage eventually exceeds the turn-on voltage, and the current bypasses through the cold diode. The cold diode is warmed up by the bypassing current, and the forward voltage of the diode decreases with the temperature rise. The reduction of the forward voltage enhances the current bypass and eventually prevents the magnet from overheating. However, the voltage increase observed in the cold tests of the first prototype magnet was slower than expected as described in the previous section. In order to re-evaluate the quench protection scheme, a numerical simulation was carried out.

1) Simulation Model: The basic equation to simulate the magnet quench is the one-dimensional thermal equilibrium

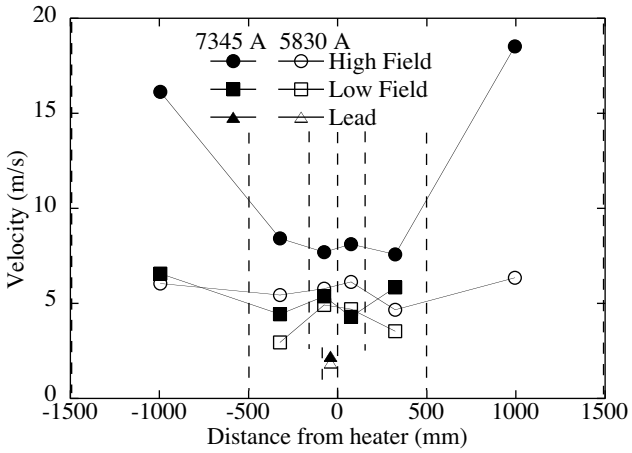

Fig. 6. Measured quench propagation velocity at the nominal current of 50 and 40 GeV.

equation as follows;

$$\frac{\partial}{\partial x}\left(\kappa(T)\frac{\partial T}{\partial x}\right) + g + p_{cn} = C(T)\frac{\partial T}{\partial t}, \tag{2}$$

where κ is the thermal conductivity, T is the temperature, g is the heat generation power per unit volume, p_{cn} is the heat conduction between the cables, and C is the specific heat. This equation is solved along the cable step by step with the Crank-Nicholson method. Other simulation conditions are as follows: the plastic spacer and G11 wedge is thermally insulated, no heat conduction between the top and bottom coils, the cold diode is connected in parallel with the magnet, and the magnet is under adiabatic conditions. The fourth condition is not actual because the magnet system will be cooled by a supercritical helium, however, such conservative assumption seems to be preferable for the purpose of the quench protection study.

2) Numerical Results: First, the simulation was carried out in the same conditions as the heater quench tests of the first prototype except for connecting the cold diode instead of the dump resistor. Fig. 7 shows the temperature profile in the magnet at 1.0 s after the quench. The quench initiates in the center of the straight section at the high field side. The normal zone does not propagate in the magnet so much, and the maximum temperature exceeds 500 K. Such high temperature is not acceptable for quench protection. It is no wonder that the peak temperature in the quench at a lower field is higher than the quench at a high field. Fig. 8 shows the current changes and maximum temperatures in the magnet. In the quench at the lower field, the quench propagation is slow and the bypass of current into the cold diode is delayed, therefore, the temperature rises steeply.

Comparison of the numerical results with the test results are shown in Fig. 9, which shows the resistive voltage of both the numerical and test results at different quench positions. The computed voltage at the higher field is much lower than the test results in spite of the adiabatic condition. These discrepancies are seemed that the conditions of computation are not optimized for the test results. However, the calculated result is in good agreement with the measured one at the lowest field, where it is the most severe region in terms

of the quench protection. The calculated temperature in that condition is over 700 K in Fig. 8. It cannot be expected that the cooling effect helps to reduce the peak temperature by several hundred Kelvin. These results indicate that the SCFM is not self protected with a cold diode.

3) Discussion of Quench Protection Scheme: Three additional quench protection options were examined by computation: a) use copper wedges in the coil straight section instead of the G11 wedges; b) cover the outside of the coil straight section with high purity aluminum sheet; and c) attach quench protection heaters, QPHs. Fig. 10 shows the current and temperature changes in the three cases of the quench at the lowest field. The maximum temperatures of Al sheets slightly decrease in comparison with the no additional protection scheme, because of the enhancement of the thermal propagation by the Al sheets. However, the temperature is still too high. In the case of Cu wedges, they do not help the peak temperature decrease at all. Meanwhile, the calculation for the quench protection heaters shows a good result. This computation was made assuming that the small sheet heater covering 21 turns in the width of 80 mm is attached to the lead end of the straight section of the top and bottom coils. The quench detector is needed for the method. The computation was made at the threshold of 0.1V, 20 ms. The peak temperature decreased to an acceptable value in terms of the magnet protection. These results show that the quench protection heater is adequate for the SCFM safe protection.

Some more simulations assuming the QPH method were carried out. Fig. 11 shows the relationship between the peak temperature and the delay from the quench initiation until the QPH causes further quench. The computations were made in the case of two QPHs and four QPHs. The former is placed at the lead end of straight section of both the top and bottom coils, and the latter is placed at both the lead and return end of the straight section of the both coils. The thermal diffusion delay the QPH through the thermal insulation is expected to be about 0.1 sec. Considering the possibility of additional delays in detecting the quench due to the electrical noise, 4 QPHs are preferable for the safe protection.

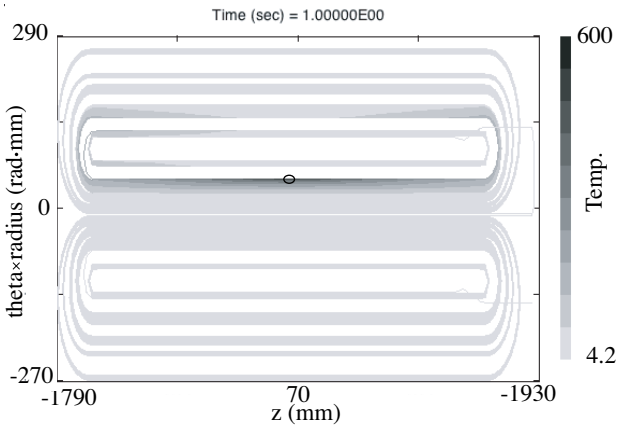

Fig. 7. The calculated temperature profile in 1.0 s after the quench. The quench initiates at the center of the straight section at the high field side, pointed by an open circle.

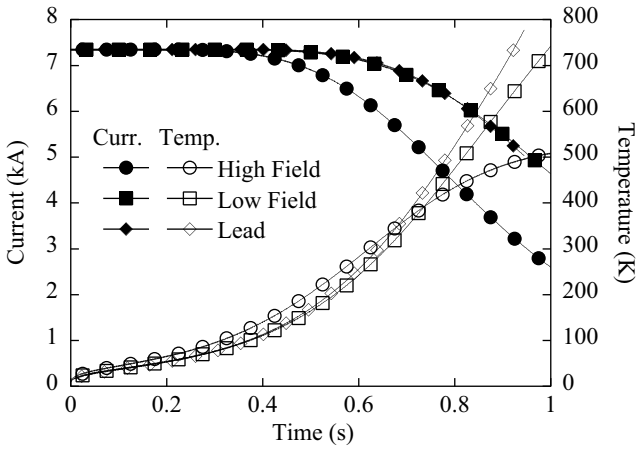

Fig. 8. The current and temperature changes in the case of the quench at the higher field, lower field and lead.

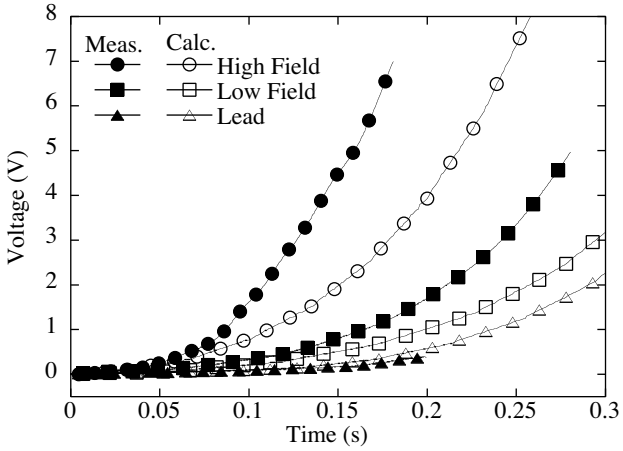

Fig. 9. The calculated and measured voltage developments at 50 GeV.

C. Test Results of the Second Prototype

The second prototype magnet has two QPHs at the lead end of the straight section in the higher field. The end spacers made of G11 were grooved with the rectangular shape in the depth of 0.3 mm, and the small sheet heaters, 66 mm wide $\times$ 44 mm height, were set in the grooves with the Kapton tape which controls the total thickness.

The important information of the QPH is the input energy required to initiate the quench. The heater covers multi-turns of the coil, and it must cause the quench in all the turns at once. Fig. 12 shows the balanced voltage rise at the different heater energies. The magnet current was 5830 A. The voltage signal with about 50 J closely resembled the signal with 63 J. It indicates that the energy density of more than 0.017 J/mm^2 is needed to initiate the quench in all the turns covered by the QPH. In these tests, the time delay from the start of the heater pulse until the quench initiation was about 0.19 s at least, which was defined by the total thickness of the thermal insulation between QPH and the cable, which was about 0.33 mm in this magnet. In the production magnets, the thickness of the insulation will be reduced to about 0.18 mm so that the time delay is expected to be about 0.1 s. As described in the previous section, the total time delay up to 0.26 s is acceptable in terms of the magnet protection, therefore, the threshold of

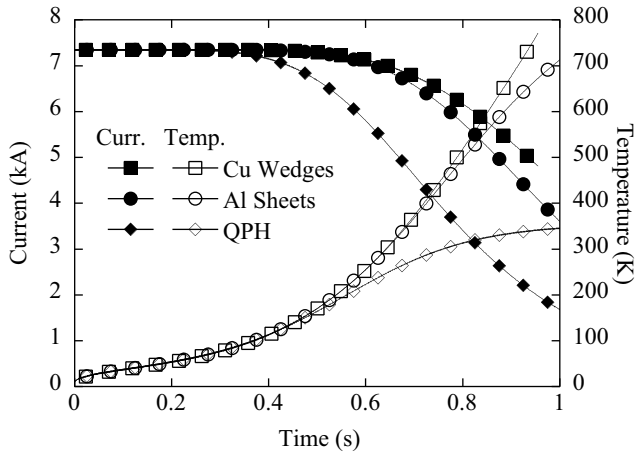

Fig. 10. The current and maximum temperature changes assuming the Al sheets, Cu wedges and quench protection heaters. The quench initiates at the lead on the median plane.

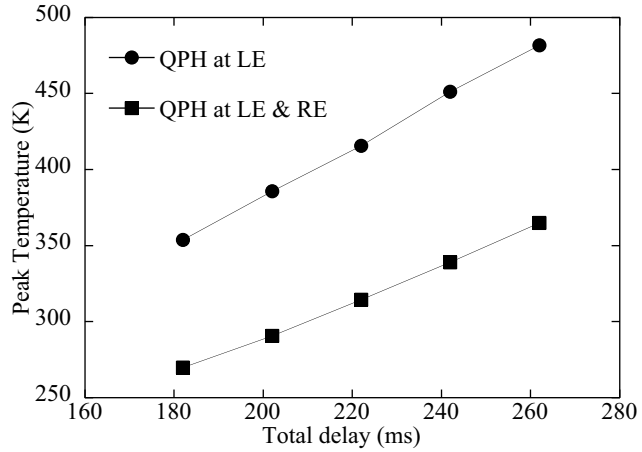

Fig. 11. The calculated peak temperature as a function of the total delay.

the quench detector can be selected conservatively.

V. Summary and Further Plan

Two full-scale prototypes of SCFMs for the primary proton beam line of the J-PARC neutrino experiment were tested at 4.2 K. In the excitation tests, both magnets were successfully energized up to 7700 A without spontaneous quenches. The first prototype magnet did not degrade at all after a thermal cycle. In the field measurement of both prototypes, the field quality in the straight section and the integrated field along the magnet axis met the specifications except for the dipole field, which was not measured precisely in the present vertical testing system. The quench heater tests of the first prototype showed that the quench propagation velocity in the lower field region was much slower than expected, and a revision of the quench protection scheme was needed. The simulation results indicated that only the quench protection heater can protect the magnet. It was also found from the

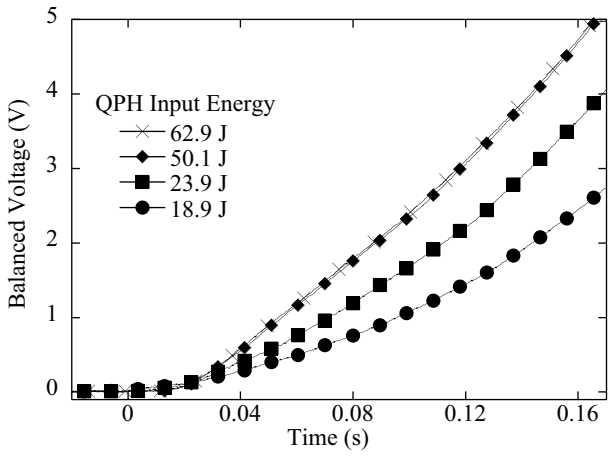

Fig. 12. The balanced voltages at different heater energies when the quench was induced by the QPH on the bottom coil.

computation that the four small QPHs were sufficient to prevent the magnet from burnout. In the second prototype magnet, quench tests using the small sheet heaters were performed, and the effective energy density of the QPH was derived from the comparison of the balanced voltages at the different heater energies.

The first prototype magnet has been disassembled after the second test, and four quench protection heaters have been attached in the identical positions to those which are planned for the production magnets. The reassembled prototype magnet will be tested again in the vertical cryostat. The two prototype magnets are to be assembled in a single cryostat system under development, and the full test will be carried out in the horizontal position in early 2006.

References

[1] Y. Itow et. al., "The JHF-Kamioka neutrino project," hep-ex/0106019.
[2] M. Furusaka, R. Hino, Y. Ikeda *et. al.*, "The joint project for high intensity proton accelerators," KEK Report 99-1; JAERI-Tech 99-056; JHF-99-3, 1999.
[3] Y. Ajima, *et al.*, "The MQXA quadrupoles for the LHC low-beta insertions," *Nucl. Inst. Method* A550(2005), 499-513.
[4] T. Nakamoto, N. Higashi, T. Ogitsu *et. al.*, "Design of Superconducting Combined Function Magnets for the 50 GeV Proton Beam Line for the J-PARC Neutrino Experiment," *IEEE Trans. on Appl. Superc.* Vol. 14, No. 2 (2004) 616 - 619.
[5] T. Ogitsu, Y. Makida, T. Kobayashi *et al.*, "Superconducting Magnet System at the 50 GeV Proton Beam Line for the J-PARC Neutrino Experiment," *IEEE Trans. on Appl. Superc.* Vol. 14, No. 2 (2004) 604 - 607.
[6] T. Nakamoto, *et al.*, "Development of a Prototype of Superconducting Combined Function Magnet for the 50 GeV Proton Beam Line for the J-PARC Neutrino Experiment," to be published in *IEEE Trans. Appl. Superconduct.*, Vol.15, 2005.
[7] T. Nakamoto, Y. Ajima, Y. Fujii *et al.*, "Development of Superconducting Combined Function Magnets for the Proton Transport Line for the J-PARC Neutrino Experiment," Proc. of Particle Accelerator Conference 2005.
[8] T. Tomaru, K. Sasaki, T. Nakamoto *et al.*, "Alignment and warm measurements of the J-PARC combined function magnets," to be presented at this conference, MOA08PO02.